Journal of Solid Mechanics Vol. 12, No. 1 (2020) pp. 16-32
DOI: 10.22034/jsm.2019.563759.1273

Vibration Analysis of Rotary Tapered Axially Functionally Graded Timoshenko Nanobeam in Thermal Environment

N. Shafiei [1], M. Hamisi [2], M. Ghadiri [1,*]

[1]*Faculty of Engineering, Department of Mechanics, Imam Khomeini International University, Qazvin, Iran*
[2]*Mechanical Engineering, Shahid Beheshti University, Tehran, Iran*

Received 2 September 2019; accepted 26 November 2019

ABSTRACT

In this paper, vibration analysis of rotary tapered axially functionally graded (AFG) Timoshenko nanobeam is investigated in a thermal environment based on nonlocal theory. The governing equations of motion and the related boundary conditions are derived by means of Hamilton's principle based on the first order shear deformation theory of beams. The solution method is considered using generalized differential quadrature element (GDQE) method. The accuracy of results are validated by other results reported in other references. The effect of various parameters such as AFG index, rate of cross section change, angular velocity, size effect and boundary conditions on natural frequencies are discussed comprehensively. The results show that with increasing angular velocity, non-dimensional frequency is increased and it depends on size effect parameter. Also, in the zero angular velocity, it can be seen with increasing AFG index, the frequencies are reducing, but in non-zero angular velocity, AFG index shows complex behavior on frequency.

Keywords: Vibration analysis; Rotary tapered nanobeam; Axially functionally graded; Timoshenko beam theory; Thermal environment.

1 INTRODUCTION

THE composites were presented among materials in order to have conflict properties such as lightness, high strength, ductility etc. Since composite materials are made up from one or more materials with distinct physical and chemical properties, these are named as advanced materials [1]. Delamination, that also called interlaminar

*Corresponding author. Tel.: +98 28 33901144 ; Fax: +98 28 33780084.
E-mail address: ghadiri@eng.ikiu.ac.ir (M.Ghadiri).

cracking, is the big problem of composites that is one type of composite materials' damage that occurs [2]. The applicable special structures are modeled by beams with non-uniform cross sectional areas like tapered beams, biomechanics, civil, robotics and mechatronics are some industrials that used this beams for the reason that arbitrary strength distribution and ability to control stress distribution in non-uniform cross sectional beams. The elastic- and rotary-types of micro and nanoelectromechanical systems (MEMS& NEMS) are more used in modern technology. Microcantilever-based contact-type sensors and actuators as well as microrotor-based devices have a huge application potential in different fields of industry including telecom, IT, material characterization, chemistry and environmental monitoring, (bio) medical, automotive, aerospace and defense applications [3]. For some micro-structures and micro-sized systems such as biosensors, atomic force microscopes and etc. can be used microbeams[4, 5]. The vibration analysis of beams considering rotary effects have been studied in different solution methods by a large number of researchers. Kaya investigated free vibration analysis of a rotating Timoshenko beam by differential transform method (DTM). Applying the TD method to the blade type rotating Timoshenko beams is accomplished by his study for the first time[6]. Dewey and Hodges used finite-element method of variable order to develop free vibration of rotating beams. Also, they explained results for uniform beams with zero and nonzero hub radius, tapered beams, and a non-uniform beam with discontinuities [7]. Many researchers studied on static and dynamic behavior analyses of microbeams recently. In this years, the different methods were used to study uniform and non-uniform microbeams. In many articles modified couple stress theory have been used for modeling behavior of materials at micro scale according to accuracy and accordance with experimental results of this theory. Chen et al. used first order shear deformation theory in developing a modified couple stress model for bending analysis of composite laminated beams [8]. According to the Euler -Bernoulli beam theory within the modified strain gradient elasticity and modified couple stress theories, Akgöz studied on bending of micro-sized beams. The boundary conditions in his study that was taken into consideration were propped cantilever, both ends clamped, both ends simply supported and cantilever cases. The conclusion of his results revealed that there is a significant difference between the bending values obtained by higher-order elasticity theories with those calculated by the classical elasticity theory [9]. Asghari et al. presented a nonlinear size-dependent Timoshenko beam model by using modified couple stress theory. Also, they used multiple scales method for analyzing the free-vibration of microbeam [10]. Challamel worked on bending of small scale rods analysis by using some simplified non-local beam theory [11]. Chen et al. studied on rotating tapered Timoshenko beams by determining natural frequencies, mode shapes and their geometrical properties varying linearly with the technique of variational iteration [12]. Dehrouyeh-Semnani used first deformation beam and modified couple stress theories for considering the influence of size effect on flap wise vibration of rotating microbeams. Also, for examining free vibration behavior of the microbeam, He developed a finite element method [13]. Yong Huang and Xian-Fang Li studied a new approach to solve natural frequencies for free vibration of axially functionally graded (AFG) tapered beams with non-uniform cross-section combined of aluminum and zirconia as two constituent phases under typical end supports including simply supported, clamped, and free ends [14]. Shojaeefard et al. investigated a comparative study on magnetic field effect on size dependent free vibration of smart rotary functionally graded nano/microplates [15]. Also they considered vibration and buckling analysis of a rotary functionally graded piezomagnetic nanoshell embedded in viscoelastic media [16] and finally focused on free vibration of an ultra-fast-rotating-induced cylindrical nano-shell resting on a Winkler foundation under thermo-electro-magneto-elastic condition [17]. Sarkar and Ganguli worked on Closed-form solutions of free vibration for axially functionally graded (AFG) Timoshenko beams having a uniform cross-section and fixed–fixed boundary condition for certain polynomial variations of the material mass density, elastic modulus and shear modulus, along the length of the beam [18]. Free vibration and stability analysis of AFG tapered Timoshenko beams are investigated by Shahba et al through a finite element approach with classical and non-classical boundary conditions [19]. Shahba and Rajasekaran studied on free vibration and stability of tapered Euler–Bernoulli beams made of AFG materials using differential transform element method (DTEM) and differential quadrature element method of lowest-order (DQEL) [20]. A new approach to the vibration behaviors of AFG Timoshenko beams with non-uniform cross-section was studied by Yong Huang and et al. An advantage of the suggested approach is that the derived characteristic equation is a polynomial equation, where the lower and higher-order natural frequencies can be determined simultaneously from the multi-roots [21]. Rajasekaran worked on the free vibration of centrifugally stiffened AFG tapered Timoshenko beams using differential transformation and quadrature methods. Natural frequencies are obtained for problems by considering the effect of material non-homogeneity, taper ratio, shear deformation parameter, rotating speed parameter, hub radius and tip mass [22]. A comprehensive review of the both analytical and numerical methods were employed by Swaminathan et al. to study the static, dynamic and stability behavior of FGM plates. The effect of variation of material properties through the thickness, type of load case, boundary conditions, edge ratio, side to thickness ratio and the effect of nonlinearity on the behavior of FGM plates were discussed [23]. Shojaeefard et al. investigated free vibration and critical angular

velocity of a rotating variable thickness two-directional FG circular microplate [24]. Free vibration and thermal buckling behavior of temperature dependent FG porous plate using modified couple stress theory based on CPT and FSDT was studied by Shojaeefard et al. [25].

In this paper, vibration analysis of rotary tapered axially functionally graded Timoshenko nanobeam is investigated in a thermal environment based on nonlocal theory. General motion equations and related boundary condition are derived by means of Hamilton's principle. The solution method is considered using generalized differential quadrature element (GDQE) method. The accuracy of results are validated by other results reported in other references.

2 THEORY AND FORMULATION OF AFG NANOBEAM EQUATIONS

Consider an axially functionally graded nanobeam with geometrical properties: length (*L*), width (*b*) and thickness variable which is made by composing two different materials (metal and ceramic) without separating boundary which means the volume fraction varies continuously (Fig.1).

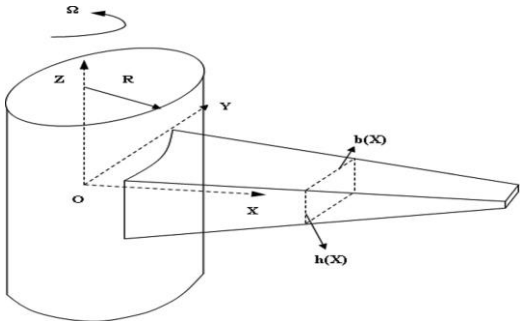

Fig.1
Configuration of axially functionally graded tapered rotating cantilever beam.

Material distribution is assumed to follow power law as following equations:

$$V_c = (x/l)^n \tag{1a}$$

$$V_m = 1 - V_c \tag{1b}$$

where V_c and V_m are volume fraction of ceramic and metal, respectively. Seeing Fig. 1, it is observed that at $x = 0$ of AFG nanobeam, the volume fraction of metal is one. By the way, the both end of the AFG nanobeam is made of pure metal and pure ceramic respectively, that ceramic percentage increases by getting closer to the $x = l$, which means at $x = l$ it is totally made of ceramic. Considering Eqs. (1) and as the function of volume fraction of AFG nanobeam.

Considering Timoshenko AFG nanobeam which is made by composing two different materials (metal and ceramic), the material and geometrical properties of the nanobeam are assumed to vary arbitrarily in the axial direction (*x*) and it can be defined as a linear function of nanobeams length (*f*(*x*)). Material and geometrical properties of the nanobeam is shown in Fig. (1) which is presented in Eqs. (1) [8].

$$F(x) = F_1 - (F_1 - F_2)\frac{x}{L} \tag{2}$$

where the subscripts 1 and 2 denote the left ($x = 0$) and the right ($x = l$) sides of the nanobeam. $F(x)$ Can be rewritten as (3) , (4) [8]:

$$F(x) = F_1(1 - f\ \frac{x}{L}) \tag{3}$$

where

$$f = (1 - \frac{F_2}{F_1}) \tag{4}$$

The material and geometrical properties of nanobeam such as Young's modulus (E), shear modulus (G), mass density (ρ), material size effect parameter (l), width (b), height (h), the second moment of cross-sectional area (I) and cross-sectional area (A) can be obtained from (1c) and (1d) [8].

From above equations, it can be seen that in the left side ($x = 0$), middle ($x = L/2$) and right side ($x = L$) cross-sectional area of AFG nanobeam, material and geometrical properties function can be written $F(x) = F_1$, $F(x) = F_1/2 + F_2/2$ and $F(x) = F_2$, respectively. It means that the left side cross-sectional area of AFG nanobeams made of pure metal, in middle cross-sectional area of AFG nanobeam the percent of volume fraction of ceramic and metal is equal to 50% of the total material and the left side cross-sectional area of AFG nanobeam is made of pure ceramic.

Mechanical and physical properties of the beam can be evaluated according to following equations:

$$\begin{aligned} E(x,T) &= E_m(x) + (E_c(x) - E_m(x))(x/l)^n \\ E_m(x) &= E_m(x=0) - (E_m(x=0) - E_m(x=L))(x/L) \\ E_c(x) &= E_c(x=0) - (E_c(x=0) - E_c(x=L))(x/L) \end{aligned} \tag{5a}$$

$$\begin{aligned} \rho(x,T) &= \rho_m(x) + (\rho_c(x) - \rho_m(x))(x/l)^n \\ \rho_m(x) &= \rho_m(x=0) - (\rho_m(x=0) - \rho_m(x=L))(x/L) \\ \rho_c(x) &= \rho_c(x=0) - (\rho_c(x=0) - \rho_c(x=L))(x/L) \end{aligned} \tag{5b}$$

$$\begin{aligned} \nu(x,T) &= \nu_m(x) + (\nu_c(x) - \nu_m(x))(x/l)^n \\ \nu_m(x) &= \nu_m(x=0) - (\nu_m(x=0) - \nu_m(x=L))(x/L) \\ \nu_c(x) &= \nu_c(x=0) - (\nu_c(x=0) - \nu_c(x=L))(x/L) \end{aligned} \tag{5c}$$

where $E(x,T)$, $\rho(x,T)$ and $\nu(x,T)$ are Young's modulus, mass density and Poisson's ratio at the certain point (x), respectively, while subscript c denotes ceramic phase and subscript m expresses properties in the metal phase. In addition, n is the power law index which determines material distribution. Need to be mentioned that Poisson's ratio is assumed to be same through the thickness and it doesn't vary along z axis. Other material properties like Lame's parameters for considered AFG nanobeam can be evaluated using Eqs. (5a), (5b). To get more accuracy of high temperature environments, it is important to consider mechanical properties variation at different temperatures. The nonlinear thermo-elastic equation can be considered to model material behavior at temperature T as [14]:

$$Y = Y_0\left(Y_{-1}T^{-1} + Y_1T + Y_2T^2 + Y_3T^3 + 1\right) \tag{6}$$

where Y_0, Y_{-1}, Y_1, Y_2 and Y_3 are the temperature dependent coefficients of material property.

2.1 Kinematic relations

The equations of motion are derived based on the Timoshenko beam theory according to which the displacement field at any point of the beam can be written as:

$$u_x(x,z,t) = u(x,t) + z\,\varphi(x,t) \tag{7a}$$

$$u_z(x,z,t) = w(x,t) \tag{7b}$$

where t is time, φ is the total bending rotation of the cross-section, and u and w are displacement components of the mid-plane along x and z directions, respectively. Therefore, according to the Timoshenko beam theory, the nonzero strains are obtained as:

$$\varepsilon_{xx} = \frac{\partial u}{\partial x} + z\,\frac{\partial \varphi}{\partial x} \tag{8a}$$

$$\gamma_{xz} = \frac{\partial w}{\partial x} + \varphi \tag{8b}$$

where ε_{xx} is normal strain and γ_{xz} is shear strain . Based on the Hamilton's principle which states that the motion of an elastic structure during the time interval $t_1 \prec t \prec t_2$ is such that the time integral of the total dynamics potential to be extreme [18], it is expressed

$$\int_{t_1}^{t_2} \delta\left(U - T + V\right) dt = 0 \tag{9}$$

Here U is strain energy, T is kinetic energy and V is potentiate energy due to external applied forces. The virtual strain energy can be calculated as:

$$\delta U = \int_V \sigma_{ij}\,\delta\varepsilon_{ij}\,dV = \int_V \left(\sigma_{xx}\,\delta\varepsilon_{xx} + \sigma_{xz}\,\delta\gamma_{xz}\right) dV \tag{10}$$

Substituting Eqs. (8) into Eq. (10) yields:

$$\delta U = \int_0^L \left(N\left(\delta\frac{\partial u}{\partial x}\right) + M\left(\delta\frac{\partial \varphi}{\partial x}\right) + Q\left(\delta\frac{\partial w}{\partial x} + \delta\varphi\right)\right) dx \tag{11}$$

In which N is the axial force, M is the bending moment and Q is the shear force. These stress resultants used in Eq. (11) are defined as:

$$N = \int_A \sigma_{xx}\,dA, \qquad M = \int_A \sigma_{xx}\,z\,dA, \qquad Q = \int_A K_S\,\sigma_{xz}\,dA \tag{12}$$

where K_S is the shear correction factor. The kinetic energy of Timoshenko beam can be written as:

$$T = \frac{1}{2}\int_0^L \int_A \rho\left(x, T\right)\left(\left(\frac{\partial u_x}{\partial t}\right)^2 + \left(\frac{\partial u_y}{\partial t}\right)^2 + \left(\frac{\partial u_z}{\partial t}\right)^2\right) dA\,dx \tag{13}$$

Also, the virtual kinetic energy can be expressed as:

$$\delta T = \int_0^L \left[\begin{array}{l} m_0\left(\dfrac{\partial u}{\partial t}\dfrac{\partial \delta u}{\partial t} + \dfrac{\partial w}{\partial t}\dfrac{\partial \delta w}{\partial t}\right) + m_1\left(\dfrac{\partial \varphi}{\partial t}\dfrac{\partial \delta u}{\partial t} + \dfrac{\partial u}{\partial t}\dfrac{\partial \delta \varphi}{\partial t}\right) \\ + m_2\left(\Omega^2\varphi\delta\varphi + \dfrac{\partial \varphi}{\partial t}\dfrac{\partial \delta \varphi}{\partial t}\right) \end{array}\right] dx \tag{14}$$

where $\left(m_0, m_1, m_2\right)$ are the mass moments of inertia defined as follows:

$$\left(m_0, m_1, m_2\right) = \int_A \rho\left(x, T\right)\left(1, z, z^2\right) dA \tag{15}$$

Now, rotation effect on the governing equation is evaluated. The variation of the work done corresponding to changes of angular velocity can be obtained by:

$$\delta V = \int_0^L \bar{N} \frac{\partial w}{\partial x} \frac{\partial \delta w}{\partial x} dx \tag{16}$$

That

$$\bar{N} = N^{Rotation} + N^{Thermal} = \int \frac{\rho(x, T)\Omega^2}{2}\left[\left(L - x\right)\left(L + 2r + x\right)\right] dA + \int E\left(x, T\right)\alpha\left(x, T\right)\left(T - T_0\right) dA \tag{17}$$

where ρ , Ω , r, x and T_0 are beam density at the certain point x, angular velocity, hub radius, beam length variation along x direction and the reference temperature. By substituting Eqs. (11), (14) and (16) into Eq. (9) and setting the coefficients of $\delta U, \delta w$ and $\delta \varphi$ to zero, the following Euler–Lagrange equation can be obtained:

$$\frac{\partial N}{\partial x} = m_0 \frac{\partial^2 u}{\partial t^2} + m_1 \frac{\partial^2 \varphi}{\partial t^2} \tag{18a}$$

$$\frac{\partial Q}{\partial x} - \bar{N} \frac{\partial^2 w}{\partial x^2} = m_0 \frac{\partial^2 w}{\partial t^2} \tag{18b}$$

$$\frac{\partial M}{\partial x} - Q = m_1 \frac{\partial^2 u}{\partial t^2} + m_2 \frac{\partial^2 \varphi}{\partial t^2} \tag{18c}$$

Under the following boundary conditions:

$$N = 0 \quad or \quad u = 0 \quad at \quad x = 0 \quad and \quad x = L \tag{19a}$$

$$Q = 0 \quad or \quad w = 0 \quad at \quad x = 0 \quad and \quad x = L \tag{19b}$$

$$M = 0 \quad or \quad \varphi = 0 \quad at \quad x = 0 \quad and \quad x = L \tag{19c}$$

2.2 The nonlocal elasticity model for AFG nanobeam

In classical continuum theories, the stress at a point is assumed to be a function of strain at that point. While the non-local continuum mechanic assumes that the stress at a point is also a function of the strains in the neighborhood of the point. Besides, the forces between atoms and internal size effect parameter are also taken into consideration in the mentioned theories. Such nonlocal model was proposed by Eringen [19-21] and Eringen and Edelen [22]. Eringen attributed the nonlocality to the atomic theory of lattice dynamics and experimental observations on phonon dispersion. According to Eringen [19,20], the nonlocal stress tensor σ atpoint x is defined as:

$$\sigma_{ij}\left(x\right) = \int_\Gamma \alpha\left(\left|x' - x\right|, \tau\right) t_{ij}\left(x'\right) d\Gamma\left(x'\right) \tag{20}$$

where $t_{ij}\left(x'\right)$ are the classical, macroscopic second Piola-Kirchhoff stresses at point x that is connected to the components of the linear strain tensor ε_{kl} as:

$$t_{ij} = C_{ijkl}\,\varepsilon_{kl} \tag{21}$$

The kernel function $K\left(\left|x'-x\right|,\tau\right)$ represents the nonlocal modulus, $\left|x'-x\right|$ is the distance (in the Euclide an norm) and τ is a material constant that depends on internal and external characteristic lengths such as the lattice spacing and wavelength, respectively. The macroscopic stress σ at point *x* in a Hookean solid is related to the strain ε at the point *x* by generalized Hooke's law [23]. τ is a constant given by:

$$\tau = \frac{e_0 a}{l} \tag{22}$$

where *a* and *l* are the internal and external characteristic lengths, respectively and e_0 indicates a material constant. For a class of physically admissible kernel, it is possible to be represented the integral constitutive relations given by Eq. (20) in an equivalent differential form as:

$$\left(1-\left(e_0 a\right)^2 \nabla^2\right)\sigma_{kl} = t_{kl} \tag{23}$$

where ∇^2 is the Laplacian operator. Thus, the scale length $e_0 a$ takes into account the size effect on the response of nanostructures. For an elastic material in the one dimensional case, the nonlocal constitutive relations may be simplified as:

For an elastic material in the one dimensional case, the nonlocal constitutive relations may be simplified as:

$$\sigma_{xx} - \left(e_0 a\right)^2 \frac{\partial^2 \sigma_{xx}}{\partial x^2} = E\,\varepsilon_{xx} \tag{24a}$$

$$\sigma_{xz} - \left(e_0 a\right)^2 \frac{\partial^2 \sigma_{xz}}{\partial x^2} = G\,\gamma_{xz} \tag{24b}$$

where σ_{xx} and σ_{xz} are the nonlocal stress and strain, respectively. *E* is Young's modulus, $G = E/2\left(1-\nu\right)$ is the shear modulus (where *v* is the Poisson's ratio). For Timoshenko nonlocal AFG beam, Eqs. (24) can be rewritten as:

$$\sigma_{xx} - \left(e_0 a\right)^2 \frac{\partial^2 \sigma_{xx}}{\partial x^2} = E\left(x,T\right)\varepsilon_{xx} \tag{25a}$$

$$\sigma_{xz} - \left(e_0 a\right)^2 \frac{\partial^2 \sigma_{xz}}{\partial x^2} = G\left(x,T\right)\gamma_{xz} \tag{25b}$$

Integrating Eqs. (25) over the beam's cross-section area, the force-strain and the moment-strain of the nonlocal AFG Timoshenko beam theory can be obtained as follows:

$$N - \left(e_0 a\right)^2 \frac{\partial^2 N}{\partial x^2} = A_{xx}\frac{\partial u}{\partial x} + B_{xx}\frac{\partial \varphi}{\partial x} \tag{26a}$$

$$M - \left(e_0 a\right)^2 \frac{\partial^2 M}{\partial x^2} = B_{xx}\frac{\partial u}{\partial x} + D_{xx}\frac{\partial \varphi}{\partial x} \tag{26b}$$

$$Q - \left(e_0 a\right)^2 \frac{\partial^2 Q}{\partial x^2} = C_{xz}\left(\frac{\partial w}{\partial x} + \varphi\right) \tag{26c}$$

In which the cross-sectional rigidities are defined as follows:

$$\left(A_{xx}, B_{xx}, D_{xx}\right) = \int_A E\left(x, T\right)\left(1, z, z^2\right) dA \tag{27a}$$

$$C_{xz} = K_S \int_A G\left(x, T\right) dA \tag{27b}$$

The explicit relation of the nonlocal normal force can be derived by substituting the second derivative of N from Eq. (18a) into Eq. (26a) as follows:

$$N = A_{xx} \frac{\partial u}{\partial x} + B_{xx} \frac{\partial \varphi}{\partial x} + \left(e_0 a\right)^2 \left(m_0 \frac{\partial^3 u}{\partial x \, \partial t^2} + m_1 \frac{\partial^3 \varphi}{\partial x \, \partial t^2} \right) \tag{28}$$

Also, the explicit relation of the nonlocal bending moment can be derived by substituting the second derivative of M from Eq. (18c) into Eq. (26b) as follows:

$$M = B_{xx} \frac{\partial u}{\partial x} + D_{xx} \frac{\partial \varphi}{\partial x} + \left(e_0 a\right)^2 \left(m_0 \frac{\partial^2 w}{\partial t^2} + m_1 \frac{\partial^3 u}{\partial x \, \partial t^2} + m_2 \frac{\partial^3 \varphi}{\partial x \, \partial t^2} + \bar{N} \frac{\partial^2 w}{\partial x^2} \right) \tag{29}$$

By substituting the second derivative of Q from Eq. (18b) into Eq. (26c), the following expression for the nonlocal shear force is derived:

$$Q = C_{xz} \left(\frac{\partial w}{\partial x} + \varphi \right) + \left(e_0 a\right)^2 \left(m_0 \frac{\partial^3 w}{\partial x \, \partial t^2} + \bar{N} \frac{\partial^3 w}{\partial x^3} \right) \tag{30}$$

The nonlocal governing equations of AFG Timoshenko nanobeam in terms of the displacement can be derived by substituting N, M and Q from Eqs. (28)-(30) into Eqs. (18) respectively, as follows:

$$A_{xx} \frac{\partial^2 u}{\partial x^2} + B_{xx} \frac{\partial^2 \varphi}{\partial x^2} + \left(e_0 a\right)^2 \left(m_0 \frac{\partial^4 u}{\partial x^2 \partial t^2} + m_1 \frac{\partial^4 \varphi}{\partial x^2 \partial t^2} \right) - m_0 \frac{\partial^2 u}{\partial t^2} - m_1 \frac{\partial^2 \varphi}{\partial t^2} = 0 \tag{31a}$$

$$C_{xz} \left(\frac{\partial^2 w}{\partial x^2} + \frac{\partial \varphi}{\partial x} \right) + \left(e_0 a\right)^2 \left(\bar{N} \frac{\partial^4 w}{\partial x^4} + m_0 \frac{\partial^4 w}{\partial x^2 \partial t^2} \right) - \frac{\partial}{\partial x} \left(\bar{N} \frac{\partial w}{\partial x} \right) - m_0 \frac{\partial^2 w}{\partial t^2} = 0 \tag{31b}$$

$$\begin{aligned} &B_{xx} \frac{\partial^2 u}{\partial x^2} + D_{xx} \frac{\partial^2 \varphi}{\partial x^2} - C_{xz} \left(\frac{\partial w}{\partial x} + \varphi \right) + m_2 \Omega^2 \varphi + \left(e_0 a\right)^2 \left(m_1 \frac{\partial^4 u}{\partial x^2 \partial t^2} + m_2 \frac{\partial^4 \varphi}{\partial x^2 \partial t^2} \right) \\ &- m_1 \frac{\partial^2 u}{\partial t^2} - m_2 \frac{\partial^2 \varphi}{\partial t^2} = 0 \end{aligned} \tag{31c}$$

3 SOLUTION METHODOLOGY

Differential quadrature method (DQM) was firstly proposed by Bellman et al. as an efficient direct method to solve partial differential equations [26, 27]. The weight coefficient which is influenced by the choice of grid points affects the accuracy of DQM results. In preliminary formulations of DQM, weight coefficients were calculated by an algebraic equation system which limited the use of large grid numbers. A simple formula was presented by Shu for

weight coefficients with practically unlimited number of grid points leading to generalized differential quadrature (GDQ) method [28]. Applications of GDQ were early limited to regular domain problems. To study the multi-domain problems, Shu and Richards developed a domain decomposition technique [29]. Based on this method, the domain of the problem is divided into a number of sub-domains or elements before discretizing each subdomain using GDQ. The domain decomposition technique using GDQ method on each sub-domain is frequently named as the DQEM [28]. A more general form of this approach includes the mapping technique, in which, a generic element is mapped onto a simple computational element. The mentioned method has the advantages of the finite element method (FEM) and GDQ and it is often referred to GDQEM [30]. Grid points describe the locations of calculating derivatives and field variables in GDQ. Derivative of a function with respect to a variable at a given node is calculated as a weighted linear sum of the function values at all nodes in the mesh line. Wang and Gu introduced DQEM to apply multi-boundary conditions by assigning two degrees of freedom to each end point for a fourth-order differential equation [31]. The DQEM method is a conventional integral quadrature method which calculates the derivative of a function approximately at any point by a linear summation of all functional values along a mesh line. Hermit type polynomials are used in DQEM instead of Lagrangian polynomials which make DQEM slightly different from the conventional DQM. The key procedure in DQM and DQEM applications lies on the determination of weighting coefficients [28] and DQM is used to discretize the governing differential equations. Four element nodes are utilized to define displacement gradient and momentum and transverse force equilibrium equations on the interelement boundary. DQEM has an advantage as a finite-element method in general geometries [32]. Due to the accurate results and convenient implementation procedure, applications of GDQM and DQEM have been widely increased in various fields of study and have been developed in recent years. GDQEM is applied here to solve the obtained governing equations. For this purpose, the following solution procedure is considered. The *r-th* order derivative of function $f\left(x_i\right)$ can be defined as [28]:

$$\left.\frac{\partial^r f\left(x\right)}{\partial x^r}\right|_{x=x_P} = \sum_{j=1}^{n} C_{ij}^{(r)} f\left(x_i\right) \tag{32}$$

That *n* is the number of grid points along *x* direction and C_{ij} can be obtained by following equations:

$$\begin{aligned} C_{ij}^{(1)} &= \frac{M\left(x_i\right)}{\left(x_i - x_j\right) M\left(x_j\right)}; \; i, j = 1,2,...,\mathrm{n} \qquad \textit{and} \qquad \mathrm{i} \neq \mathrm{j} \\ C_{ij}^{(1)} &= -\sum_{j=1, i \neq j}^{n} C_{ij}^{(1)}; \qquad\qquad\qquad\qquad\qquad\quad i = j \end{aligned} \tag{33}$$

where $M(x)$ is defined as:

$$M\left(x_i\right) = \prod_{j=1, j \neq i}^{n} \left(x_i - x_j\right) \tag{34}$$

The weighting coefficient along *x* direction $C^{(r)}$ can be obtained as:

$$\begin{aligned} C_{ij}^{(r)} &= r\left[C_{ij}^{(r-1)} C_{ij}^{(1)} - \frac{C_{ij}^{(r-1)}}{\left(x_i - x_j\right)}\right]; \; i, j = 1,2,...,\mathrm{n}, \mathrm{i} \neq \mathrm{j} \qquad \textit{and} \qquad 2 \leq \mathrm{r} \leq \mathrm{n}-1 \\ C_{ii}^{(r)} &= -\sum_{j=1, i \neq j}^{n} C_{ij}^{(r)}; \qquad\qquad i, j = 1,2,...,\mathrm{n} \qquad \textit{and} \qquad 1 \leq \mathrm{r} \leq \mathrm{n}-1 \end{aligned} \tag{35}$$

To obtain a better distribution for mesh points, Chebyshev-Gauss-Lobatto technique is applied as:

$$x_i = \frac{L}{2el}\left(1-\cos\left(\frac{(i-1)}{(N-1)}\pi\right)\right) \qquad i = 1,2,3,\ldots,n \tag{36}$$

"el" refers to the number of element along the length of the microbeam. Considering "$u=Ue^{i\omega t}$, $w=We^{i\omega t}$, $\varphi=\emptyset e^{i\omega t}$ "and using GDQE method, governing equations can be rewritten as:

$$\left\{\begin{array}{l}\sum_{k=1}^{n_i} C_{i,k}^{(1)}\left(A_{xx}\sum_{k=1}^{n_i} C_{i,k}^{(1)}U_i\right)+\sum_{k=1}^{n_i} C_{i,k}^{(1)}\left(B_{xx}\sum_{k=1}^{n_i} C_{i,k}^{(1)}\phi_i\right)\\ =\omega^2\left[m_0U_i+m_1\phi_i-(e_0a)^2\sum_{k=1}^{n_i} C_{i,k}^{(2)}\left(m_0U_i+m_1\phi_i\right)\right]\end{array}\right\}_{el} \tag{37a}$$

$$\left\{\begin{array}{l}\sum_{k=1}^{n_i} C_{i,k}^{(1)}\left(B_{xx}\sum_{k=1}^{n_i} C_{i,k}^{(1)}U_i\right)+\sum_{k=1}^{n_i} C_{i,k}^{(1)}\left(D_{xx}\sum_{k=1}^{n_i} C_{i,k}^{(1)}\phi_i\right)-C_{xz}\left(\phi_i+\sum_{k=1}^{n_i} C_{i,k}^{(1)}W_i\right)\\ m_2\Omega^2\phi_i=\omega^2\left[m_1U_i+m_2\phi_i-(e_0a)^2\sum_{k=1}^{n_i} C_{i,k}^{(2)}\left(m_1U_i+m_2\phi_i\right)\right]\end{array}\right\}_{el} \tag{37b}$$

$$\left\{\begin{array}{l}\sum_{k=1}^{n_i} C_{i,k}^{(1)}\left[C_{xz}\left(\phi_i+\sum_{k=1}^{n_i} C_{i,k}^{(1)}W_i\right)\right]+\sum_{k=1}^{n_i} C_{i,k}^{(1)}\left(N^R\sum_{k=1}^{n_i} C_{i,k}^{(1)}W_i\right)\\ -(e_0a)^2\sum_{k=1}^{n_i} C_{i,k}^{(2)}\left(\sum_{k=1}^{n_i} C_{i,k}^{(1)}\left(N^R\sum_{k=1}^{n_i} C_{i,k}^{(1)}W_i\right)\right)=\omega^2\left[m_0W_i-(e_0a)^2\sum_{k=1}^{n_i} C_{i,k}^{(2)}W_i\right]\end{array}\right\}_{el} \tag{37c}$$

In Eqs. (37), the subscript *el* refers to the number of element along the length of the microbeam. In order to solve the governing equations coupling with the boundary conditions, the following matrix equation can be evaluated [33]. Finally, with solving the eigenvalue problem, the natural frequencies are obtained [28].

$$\left(\begin{bmatrix}[K_{dd}] & [K_{db}]\\ [K_{bd}] & [K_{bb}]\end{bmatrix}\begin{Bmatrix}\lambda_d\\ \lambda_b\end{Bmatrix}=\omega^2\begin{bmatrix}[M_{dd}] & [M_{db}]\\ [M_{bd}] & [M_{bb}]\end{bmatrix}\begin{Bmatrix}\lambda_d\\ \lambda_b\end{Bmatrix}\right)_{el} \tag{38}$$

4 RESULTS

In order to have better judgment on results, non-dimensional parameters are defined as following:

$$\begin{array}{ll} x=\xi L; & r=\delta L\\ \Phi^2=\left(\frac{m_0}{EI}\right)_{ceramic}L^4\Omega^2; & \Psi^2=\left(\frac{m_0}{EI}\right)_{ceramic}L^4\omega^2\\ \left(\frac{m_0}{EI}\right)_{ceramic}=\frac{12\rho_{ceramic}}{E_{ceramic}h_1^{\,2}}; & \mu=\frac{e_0a}{L}\end{array} \tag{39}$$

The coefficients of Young's modulus, mass density and Poisson's ratio have been considered in Table 1.

Comparison of results for non-dimensional angular velocity (Φ) of cantilever non-FG nanobeam for $\delta=\mu=0$ is computed and are shown in Table 2.

In Table 3., it is seen the comparison of results for non-dimensional frequency of non-uniform propped cantilever nanobeam.

Table 1
The coefficients of Young's modulus, mass density and Poisson's ratio[34].

Material	Properties	Value
SUS304	E (Pa)	2.0104e+11
	ρ (Kg/m^3)	8166
	N	0.3262
Al_2O_3	E (Pa)	3.4955e+11
	ρ (Kg/m^3)	3800
	N	0.24

Table 2
Comparison of results for non-dimensional angular velocity (Φ) of cantilever non-FG nanobeam for δ= μ =0.

Non-dimensional angular velocity (Φ)	Fundamental frequency		Second frequency	
	Present GDQM	[35]	Present GDQM	[35]
0	3.516009	3.5160	22.03437	22.035
1	3.681644	3.6816	22.18089	22.181
2	4.137318	4.1373	22.6148	22.615
3	4.797271	4.7973	23.32015	23.320
4	5.584995	5.5850	24.27323	24.273
5	6.449537	6.4495	25.44596	25.446
6	7.360362	7.3604	26.80896	26.809
7	8.299625	8.2996	28.33396	28.334
8	9.25682	9.2568	29.99526	29.995
9	10.22567	10.226	31.77039	31.771
10	11.20232	11.202	33.64024	33.640

Table 3
Comparison of results for non-dimensional frequency of non-uniform propped cantilever nanobeam.

Rate of Cross section change, (β_h)	Φ=0, Ψ_1		Φ=0, Ψ_2	
	Present GDQM	[35]	Present GDQM	[35]
0	15.41814697	15.4182	49.96433188	49.9648
0.1	14.84884477	14.8488	47.63657636	47.6370
-0.1	15.96864263	15.9687	52.23662242	52.2372
-0.2	16.50282404	16.5028	54.46077893	54.4614

As was observed, Tables 2 and 3, respectively, compared cantilever and propped cantilever nanobeam results. They showed a good agreement are consistent with the results presented with the results reported in reference [32]. As other validation, Table 4. is computed fundamental and 2nd frequency of present Timoshenko beam in deferent μ from 0 to 0.5 and then compared with Euler-Bernoulli beam and Timoshenko beam in reference [36].

Table 4
The results comparison of 1st & 2nd frequency in deferent μ for both cantilever and propped cantilever nanobeam.

	Fundamental Frequency			Second Frequency		
	Present Timoshenko	Timoshenko [36]	Euler-Bernoulli [36]	Present Timoshenko	Timoshenko [36]	Euler-Bernoulli [36]
			Propped Cantilever			
$N\mu$=0	3.921886032	3.7845	3.9266	7.045365614	6.4728	7.0686
$N\mu$=0.1	3.816364505	3.6939	3.8209	6.444224694	6.0348	6.4649
$N\mu$=0.3	3.279111326	3.2115	3.2828	4.751908019	4.6013	4.7668
$N\mu$=0.5	2.786800818	2.7471	2.7899	3.82054622	3.7312	3.8325
			Cantilever			
$N\mu$=0	1.87191249	1.861	1.8751	4.639805283	4.4733	4.6941
$N\mu$=0.1	1.875878373	1.865	1.8792	4.494033199	4.3506	4.5475
$N\mu$=0.3	1.911173814	1.8999	1.9154	3.721925038	3.6594	3.7665
$N\mu$=0.5	2.015010821	2.0024	2.0219	2.915170763	2.8903	2.9433

Independent of size effect parameter, it can be seen that frequencies are reduced. In Fig. 2 fundamental frequency is shown for cantilever nanobeam when $\beta_h=\delta=0$ in 4 states.

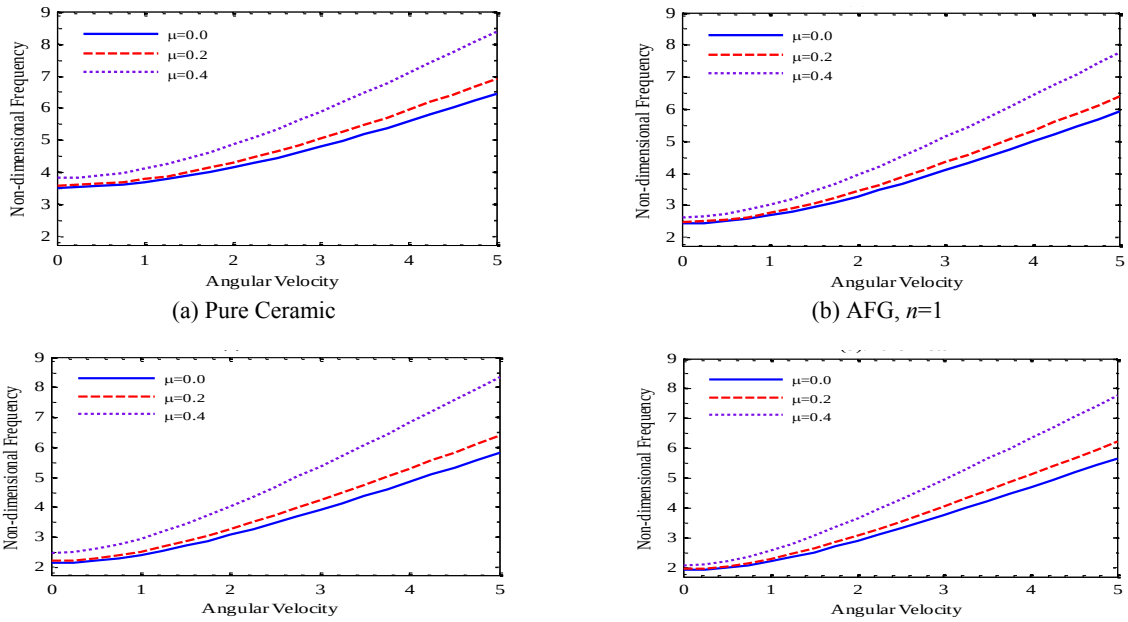

(a) Pure Ceramic (b) AFG, n=1

(c) AFG, n=5 (d) Pure Metal

Fig.2
Fundamental frequency, cantilever, $\beta_h=\delta=0$.

with increasing angular velocity, non-dimensional frequency is increased and it depends on size effect parameter. With increase of nonlocal parameter, the value of frequencies increase. In the zero angular velocity, it can be seen with increasing AFG index, the frequencies are reducing, but in non-zero angular velocity, AFG index shows complex behavior on frequency.

In Fig. 3 the second frequency is shown for cantilever nanobeam when $\beta_h=\delta=0$ in 4 states.

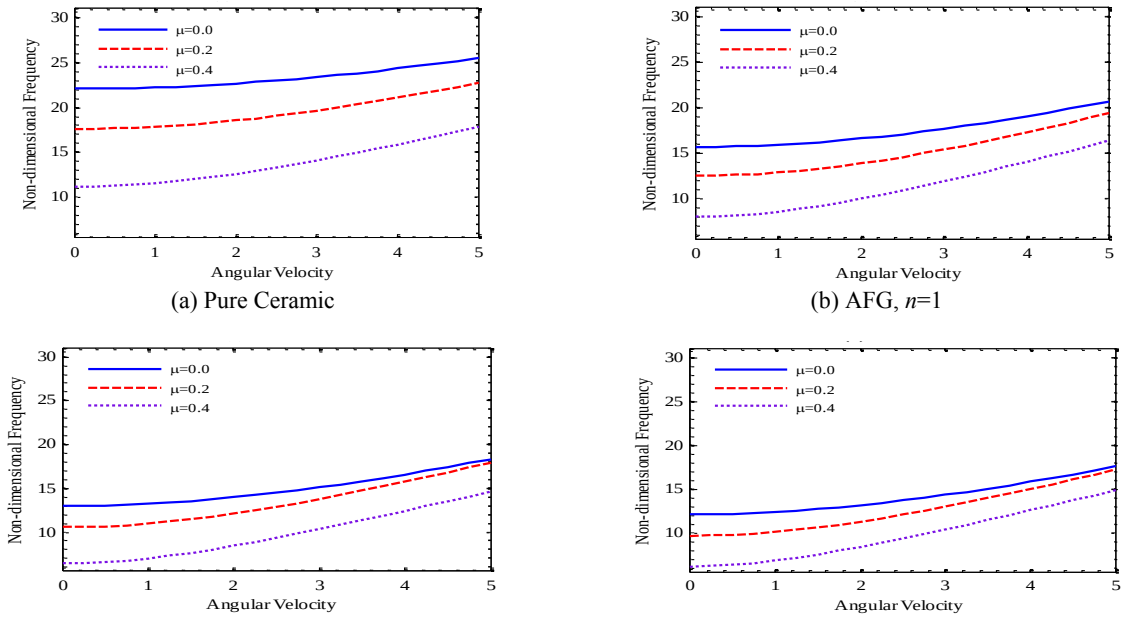

(a) Pure Ceramic (b) AFG, n=1

(c) AFG, n=5 (d) Pure Metal

Fig.3
Second frequency, cantilever, $\beta_h=\delta=0$.

In most AFG index, with all angular velocity, the frequency decreases. With increasing size effect parameter, the difference between the first and second frequencies from each other become less. It is seen that with increasing angular velocity, frequency increase and converges to one side. It means that in high angular velocity, second frequency is less dependent on size effect parameter.

The problem of interest is a rotary microbeam whose length 'L', beam height '$h = h_1\left(1+\beta_h x\right)$' and beam width '$b = b_1\left(1+\beta_b x\right)$' are located on x, z and y directions, respectively, also, $\beta_h = 1-h_2/h_1$ and $\beta_b = 1-b_2/b_1$, also, the geometrical properties of microbeam such as second moment of cross-sectional area (I) and cross-sectional area (A) can be given as, respectively:

$$I(x) = \int_{-\frac{h}{2}}^{\frac{h}{2}} \int_{-\frac{b}{2}}^{\frac{b}{2}} z^2 dy dz \tag{40a}$$

$$A(x) = \int_{-\frac{h}{2}}^{\frac{h}{2}} \int_{-\frac{b}{2}}^{\frac{b}{2}} dy dz \tag{40b}$$

In Fig. 4 the fundamental frequency is shown for cantilever nanobeam when δ=0 in 4 states.

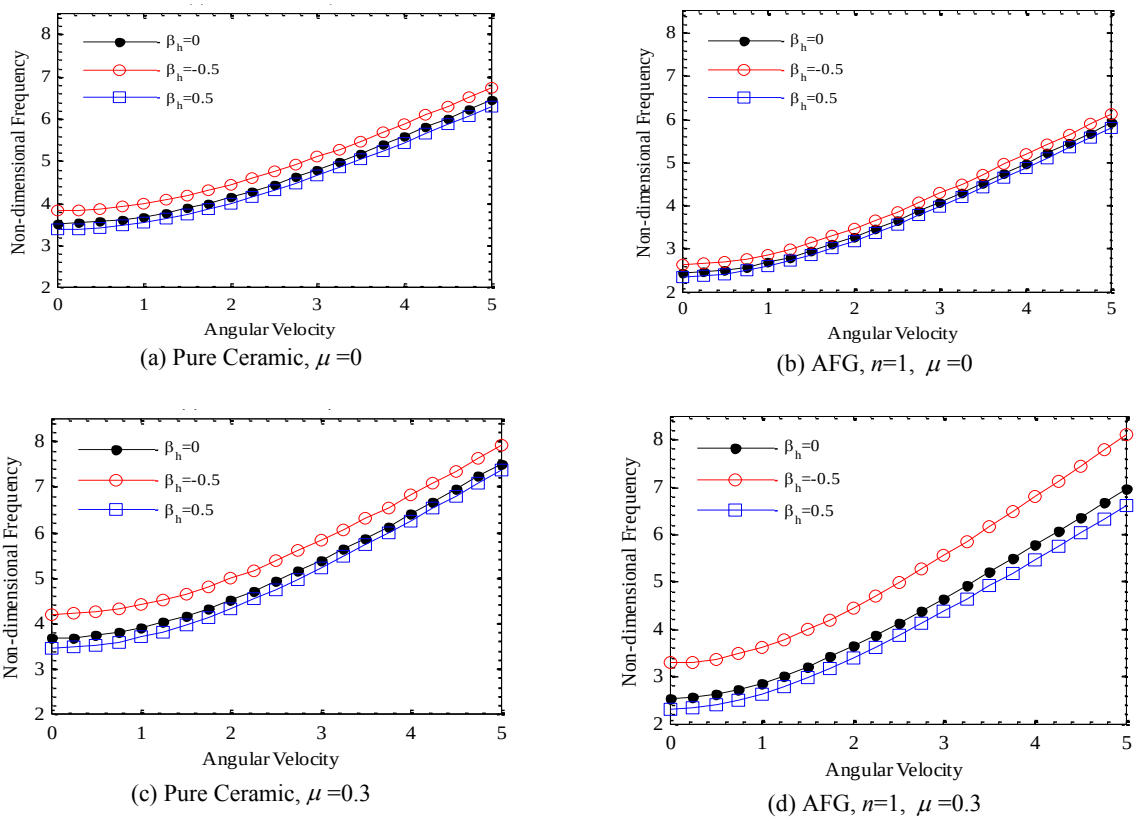

(a) Pure Ceramic, μ =0

(b) AFG, n=1, μ =0

(c) Pure Ceramic, μ =0.3

(d) AFG, n=1, μ =0.3

Fig.4
Fundamental frequency, cantilever, δ=0.

Now, we examine the effect of taper effect. In pure ceramics, geometrical changes and size effect parameter has little effect. On the other in AFG material, geometry effect is increased by increasing the size effect parameter.

In Fig. 5 the second frequency is shown for cantilever nanobeam when δ=0 in 4 states.

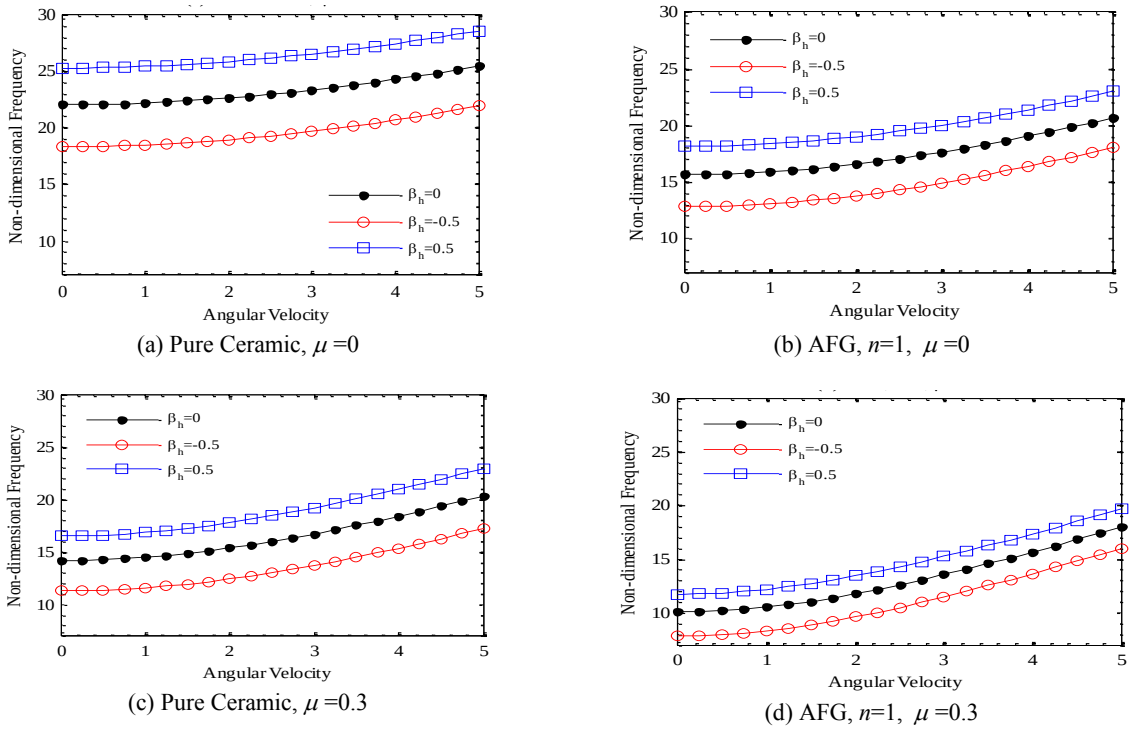

(a) Pure Ceramic, μ =0

(b) AFG, n=1, μ =0

(c) Pure Ceramic, μ =0.3

(d) AFG, n=1, μ =0.3

Fig.5
Second frequency, cantilever, δ=0.

As shown, the taper effect in second frequency is more than fundamentally frequency. After it, in Fig. 6, the fundamental frequency is shown for propped cantilever nanobeam when β_h =δ=0 in 4 states.

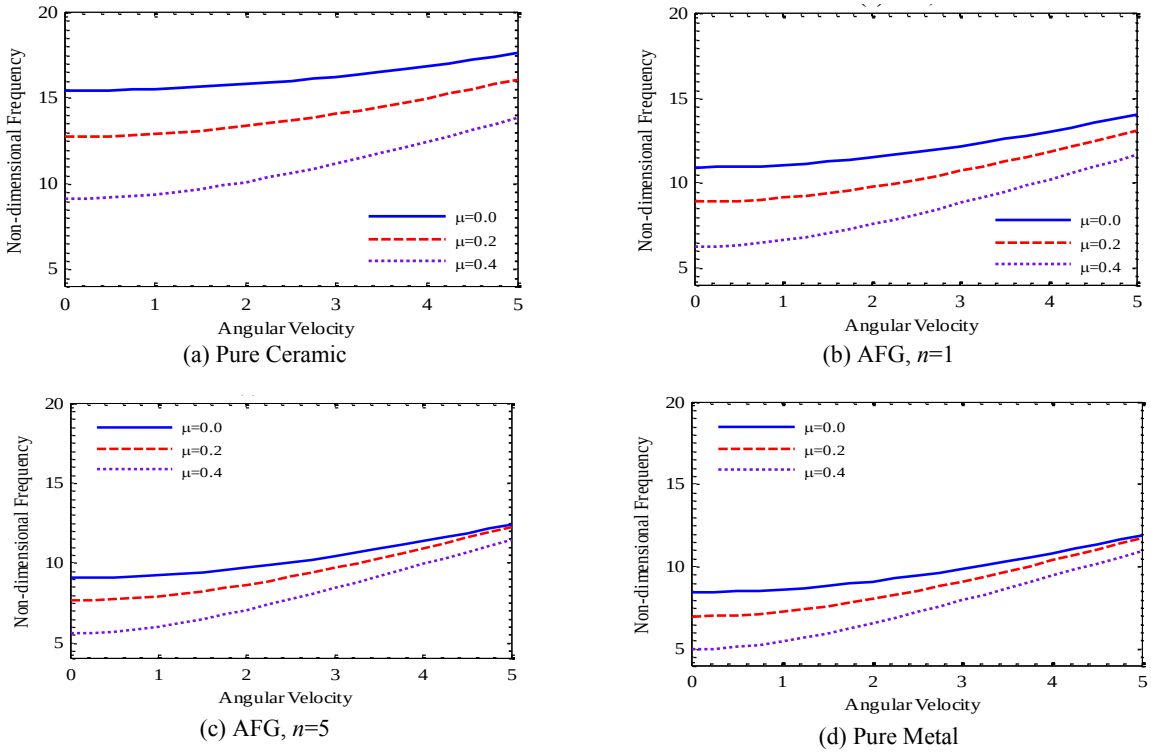

(a) Pure Ceramic

(b) AFG, n=1

(c) AFG, n=5

(d) Pure Metal

Fig.6
Fundamental frequency, propped cantilever, β_h=δ=0.

In Fig. 7 the second frequency is shown for propped cantilever nanobeam when $\beta_h = \delta = 0$ in 4 states.

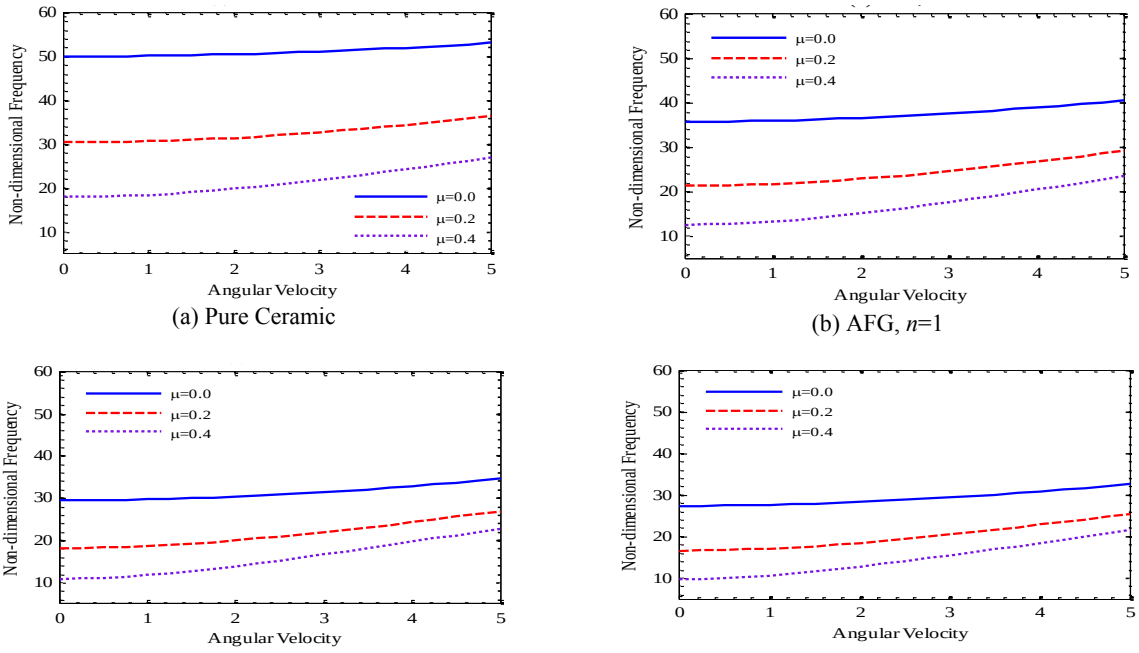

(a) Pure Ceramic (b) AFG, n=1

(c) AFG, n=5 (d) Pure Metal

Fig.7
Second frequency, propped cantilever, $\beta_h = \delta = 0$.

According to Figs. 6 and 7, with increasing AFG index, the frequency is decreased. While with the increasing of angular velocity, the frequency is increased but the effect of size effect parameter is reduced. It was also observed, the effect of size parameter in pure ceramic is far more than pure metal.

In Fig. 8 the fundamental frequency is shown for propped cantilever nanobeam when $\delta = 0$ in 4 states.

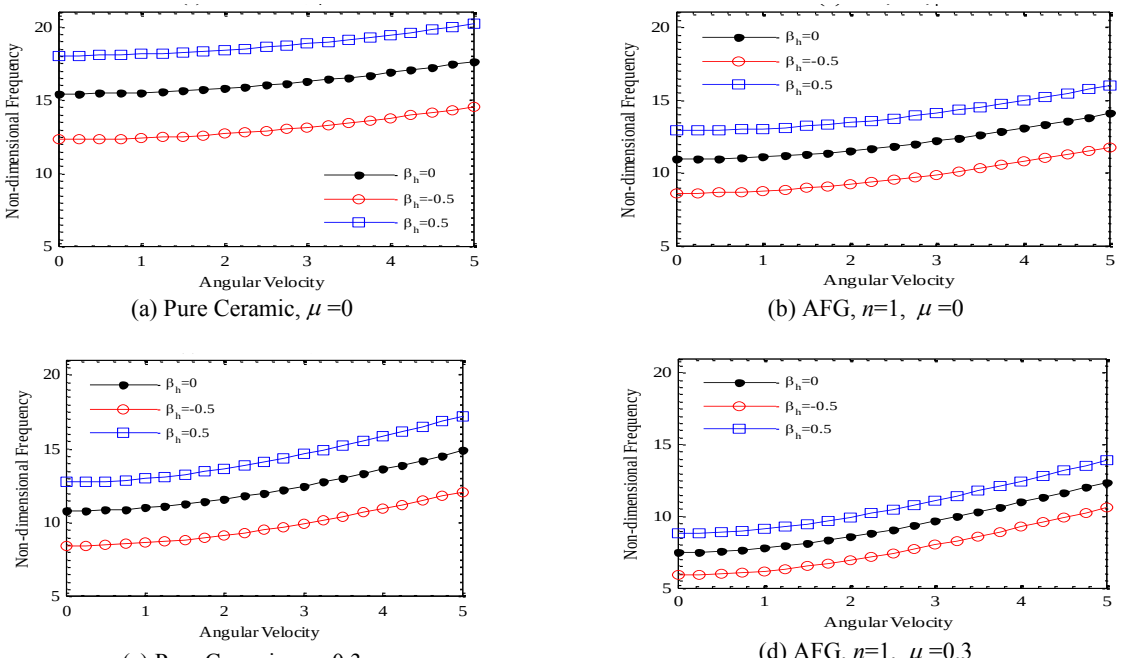

(a) Pure Ceramic, μ =0 (b) AFG, n=1, μ =0

(c) Pure Ceramic, μ =0.3 (d) AFG, n=1, μ =0.3

Fig.8
Fundamental frequency, propped cantilever, δ=0.

In Fig. 9 the second frequency is shown for propped cantilever nanobeam when δ=0 in 4 states.

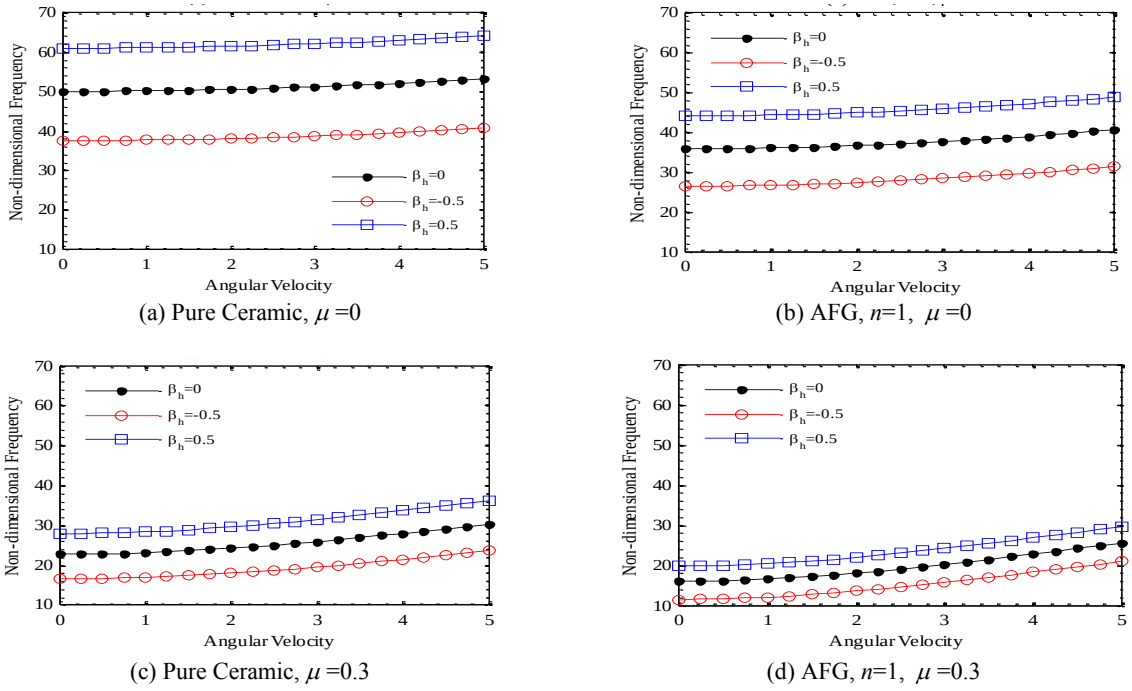

(a) Pure Ceramic, μ =0 (b) AFG, n=1, μ =0

(c) Pure Ceramic, μ =0.3 (d) AFG, n=1, μ =0.3

Fig.9
Second frequency, propped cantilever, δ=0.

According to Figs. 6 and 7, the tapered effect in second frequency is more than fundamentally frequency.

5 CONCLUSION

In this paper, vibration analysis of rotary tapered axially functionally graded Timoshenko nanobeam is investigated in a thermal environment based on non local theory. The solution method is considered using generalized differential quadrature element (GDQE) method. The accuracy of results are validated by other results reported in other references. According to obtained results, it is observed that with increasing AFG index, the frequency is decreased. While with the increasing of angular velocity, the frequency is increased but the effect of size effect parameter is reduced. It was also obtained the effect of size parameter in pure ceramic is far more than pure metal.

REFERENCES

[1] Rasheedat M., 2012, Functionally graded material: An overview, *Proceedings of the World Congress on Engineering*.
[2] Wang S.S., 1983, Fracture mechanics for delamination problems in composite materials, *Journal of Composite Materials* **17**: 210-223.
[3] Vytautas Ostasevicius R.D., 2011, Microsystems dynamics, *International Series on Intelligent Systems, Control, and Automation: Science and Engineering*.
[4] Li X.B.B., Takashima K., Baek C.W., Kim Y.K., 2003, Mechanical characterization of micro/nanoscale structures for MEMS/NEMS applications using nanoindentation techniques, *Ultramicroscopy* **97**: 481-494.
[5] Pei J.T.F., Thundat T., 2004, Glucose biosensor based on the microcantilever, *Analytical Chemistry* **76**: 292-297.
[6] Kaya M.O., 2006, Free vibration analysis of a rotating Timoshenko beam by differential transform method, *Aircraft Engineering and Aerospace Technology* **78**:194-203.
[7] Dewey H., Hodges M.J.R., 1981, Free-vibration analysis of rotating beams by a variable-order finite-element method, *AIAA Journal* **19**: 1459-1466.
[8] Chen W.L.L., Ma X., 2011, A modified couple stress model for bending analysis of composite laminated beams with first order shear deformation, *Composite Structures* **93**: 2723-2732.

[9] Akgöz B.C.Ö., 2012, Analysis of micro-sized beams for various boundary conditions based on the strain gradient elasticity theory, *Archive of Applied Mechanics* **82**: 423-443.
[10] Asghari M. Kahrobaiyan M.H., Ahmadian M.T., 2010, A nonlinear Timoshenko beam formulation based on the modified couple stress theory, *Engineering Science* **48**: 1749-1761.
[11] Challamel N.,Wang.C.M., 2008, The small length scale effect for a non-local cantilever beam: a paradox solved, *Nanotechnology* **19**: 345703.
[12] Chen Y.Z.J., Zhang H., 2015, Free vibration analysis of rotating tapered Timoshenko beams via variational iteration method, *Vibration and Control* **2015**: 1-15.
[13] Dehrouyeh-Semnani A., 2015, The influence of size effect on flapwise vibration of rotating microbeams, *International Journal of Engineering Science* **94**: 150-163.
[14] Yong H., Xian-Fang L., 2010, A new approach for free vibration of axially functionally graded beams with non-uniform cross-section, *Journal of Sound and Vibration* **329**: 2291-2303.
[15] Shojaeefard M. H., 2018, Magnetic field effect on free vibration of smart rotary functionally graded nano/microplates: A comparative study on modified couple stress theory and nonlocal elasticity theory, *Journal of Intelligent Material Systems and Structures* **29**(11): 2492-2507.
[16] Shojaeefard M.H., 2018, Vibration and buckling analysis of a rotary functionally graded piezomagnetic nanoshell embedded in viscoelastic media, *Journal of Intelligent Material Systems and Structures* **29**(11): 2344-2361.
[17] Shojaeefard M.H., 2018, Free vibration of an ultra-fast-rotating-induced cylindrical nano-shell resting on a Winkler foundation under thermo-electro-magneto-elastic condition, *Applied Mathematical Modelling* **61**: 255-279.
[18] Korak S., Ranjan G., 2014, Closed-form solutions for axially functionally gradedTimoshenko beams having uniform cross-section and fixed–fixed boundary condition,*Composites: Part B* **58**: 361-370.
[19] Shahba A., Attarnejad R., Tavanaie Marvi M., Hajilar S., 2011, Free vibration and stability analysis of axially functionally graded tapered Timoshenko beams with classical and non-classical boundary conditions, *Composites: Part B* **42**: 801-808.
[20] Shahba A., Sundaramoorthy R., 2012, Free vibration and stability of tapered Euler–Bernoulli beams made of axially functionally graded materials, *Applied Mathematical Modelling* **36**: 3094-3111.
[21] Yong H., Ling-E Y., Qi-Zhi L., 2013, Free vibration of axially functionally graded Timoshenko beams with non-uniform cross-section, *Composites: Part B* **45**: 1493-1498.
[22] Sundaramoorthy R., 2013, Free vibration of centrifugally stiffened axially functionally graded tapered Timoshenko beams using differential transformation and quadrature methods, *Applied Mathematical Modelling* **37**: 4440-4463.
[23] Swaminathan K., Naveenkuma D.T., Zenkour A. M., Carrera E., 2014, Stress, vibration and buckling analyses of FGM plates—A stateof-the-art review, *Composite Structures* **120**: 10-31.
[24] Shojaeefard M.H. , Saeidi Googarchin H., Mahinzare M., Ghadiri M. 2018, Free vibration and critical angular velocity of a rotating variable thickness two-directional FG circular microplate, *Microsystem Technologies* **24**: 1525-1543.
[25] Shojaeefard M.H. , Saeidi Googarchin H., Ghadiri M., Mahinzare M., 2017, Micro temperature-dependent FG porous plate: Free vibration and thermal buckling analysis using modified couple stress theory with CPT and FSDT, *Applied Mathematical Modelling* **50**: 633-655.
[26] Bellman R., Casti J., 1971, Differential quadrature and long-term integration, *Journal of Mathematical Analysis and Applications* **34**: 235-238.
[27] Bellman R., Kashef B., Casti J., 1972, Differential quadrature: a technique for the rapid solution of nonlinear partial differential equations, *Journal of Computational Physics* **10**: 40-52.
[28] Shu C., 2000, *Differential Quadrature and its Application in Engineering*, Springer.
[29] Shu C., Richards B.E., 1992, Application of generalized differential quadrature to solve two-dimensional incompressible Navier-Stokes equations, *International Journal for Numerical Methods in Fluids* **15**: 791-798.
[30] Viola E., Miniaci M., Fantuzzi N., Marzani A., 2015, Vibration analysis of multi-stepped and multi-damaged parabolic arches using GDQ, *Curved and Layered Structures* **2**: 28-49.
[31] Wang X., GU H., 1997, Static analysis of frame structures by the differential quadrature element method, *International Journal for Numerical Methods in Engineering* **40**: 759-772.
[32] Chen C.-N., 1998, Solution of beam on elastic foundation by DQEM, *Journal of Engineering Mechanics* **124**: 3509-3526.
[33] Shahba A., Attarnejad R., Hajilar S., 2013, A mechanical-based solution for axially functionally graded tapered Euler-Bernoulli beams, *Mechanics of Advanced Materials and Structures* **20**: 696-707.
[34] Yang J., Shen H.-S., 2002, Vibration characteristics and transient response of shear-deformable functionally graded plates in thermal environments, *Journal of Sound and Vibration* **255**: 579-602.
[35] Shafiei N., Kazemi M., Ghadiri M., 2015, On size-dependent vibration of rotary axially functionally graded microbeam, *International Journal of Engineering Science* **101**: 29-44.
[36] Wang C., Zhang Y., He X., 2007, Vibration of nonlocal Timoshenko beams, *Nanotechnology* **18**: 105401.